

Spectral mixing formulations for van der Waals–London dispersion interactions between multicomponent carbon nanotubes

Rick Rajter,^{1,a)} Roger H. French,² Rudi Podgornik,³ W. Y. Ching,⁴ and V. Adrian Parsegian⁵

¹*Department of Materials Science and Engineering, Massachusetts Institute of Technology, Room 13-5046 Cambridge, Massachusetts 02139, USA*

²*DuPont Co. Central Research, Experimental Station, E400-5207 Wilmington, Delaware 19880, USA*

³*Faculty of Mathematics and Physics, University of Ljubljana, Ljubljana, Slovenia and Department of Theoretical Physics, J. Stefan Institute, SI-1000 Ljubljana, Slovenia*

⁴*Department of Physics, University of Missouri-Kansas City, Kansas City, Missouri, 64110, USA*

⁵*Laboratory of Physical and Structural Biology, NICHD, National Institutes of Health, Bldg. 9, Room 1E116, Bethesda, Maryland 20892-0924, USA*

(Received 9 April 2008; accepted 27 June 2008; published online 10 September 2008)

Recognition of spatially varying optical properties is a necessity when studying the van der Waals–London dispersion (vdW-Ld) interactions of carbon nanotubes (CNTs) that have surfactant coatings, tubes within tubes, and/or substantial core sizes. The ideal way to address these radially dependent optical properties would be to have an analytical add-a-layer solution in cylindrical coordinates similar to the one readily available for the plane-plane geometry. However, such a formulation does not exist nor does it appear trivial to be obtained exactly. The best and most pragmatic alternative for end-users is to take the optical spectra of the many components and to use a spectral mixing formulation so as to create effective solid-cylinder spectra for use in the far-limit regime. The near-limit regime at “contact” is dominated by the optical properties of the outermost layer, and thus no spectral mixing is required. Specifically we use a combination of a parallel capacitor in the axial direction and the Bruggeman effective medium in the radial direction. We then analyze the impact of using this mixing formulation upon the effective vdW-Ld spectra and the resulting Hamaker coefficients for small and large diameter single walled CNTs (SWCNTs) in both the near- and far-limit regions. We also test the spectra of a $[16,0,s+7,0,s]$ multiwalled CNT (MWCNT) with an effective MWCNT spectrum created by mixing its $[16,0,s]$ and $[7,0,s]$ SWCNT components to demonstrate nonlinear coupling effects that exist between neighboring layers. Although this paper is primarily on nanotubes, the strategies, implementation, and analysis presented are applicable and likely necessary to any system where one needs to resolve spatially varying optical properties in a particular Lifshitz formulation. © 2008 American Institute of Physics. [DOI: [10.1063/1.2975207](https://doi.org/10.1063/1.2975207)]

I. INTRODUCTION

Single walled carbon nanotubes (SWCNTs) are a unique class of materials with chirality-dependent electronic properties,^{1–4} optical properties,^{5–7} and van der Waals–London dispersion (vdW-Ld) energies/forces.^{5,8,9} Numerous experimental procedures have exploited the differences among these properties in order to separate SWCNTs by chirality,^{10–14} which is a necessary step to create workable nanodevices that need a particular band gap or set of electronic conduction properties. The ultimate goal is to be able to reliably separate this mixed “pasta” of SWCNTs in solution into monodisperse populations of one chirality for commercial/industrial use. To achieve this goal, new strategies and a more rigorous understanding of the fundamental forces are needed.

II. BACKGROUND

The study of vdW-Ld forces for SWCNT systems was primarily motivated by the 2003 experiments of Zheng *et al.*,¹⁰ where consistent and significant progress was made in

separating metallic and semiconducting CNTs using ion exchange chromatography (IEC) with a time-varying salt concentration. In short, SWCNTs produced by the high-pressure CO (HiPCO) method were wrapped with single-stranded DNA (ssDNA) of a specific length and base pair sequence (50 base pairs of alternating guanine thymine) as a surfactant to isolate single tubes in an aqueous solution. These collections of ssDNA/SWCNT hybrids, which contained a mixture of many different chiralities, were then injected into the anion IEC column in order to trap them onto the highly charged beads. Next, the concentration of sodium thiocyanate salt was slowly increased to screen out the strong electrostatic forces that bind the hybrids to the charged beads inside the column. This systematic increase in the charge screening caused the SWCNTs to be released as a function of their initial binding strength, which were then carried out and collected into a series of vials.

The experiments of Zheng *et al.*¹⁰ were consistently repeatable. The initial samples that eluted were always predominantly enriched in the metallic chiralities. However, the exact mechanism or collection of mechanisms/interactions responsible for this separation has still not been conclusively settled. There are at least three possibilities for the selectiv-

^{a)}Electronic mail: rickrajter@alum.mit.edu.

ity: (A) Each SWCNT chirality has a preferred ssDNA wrapping configuration that presumably maximizes the interaction between the ssDNA base pairs and the underlying sp^2 carbon bonds. This results in a chirality-dependent surface charge density because the wrapping configuration determines the number of the negatively charged phosphates per unit area of SWCNT surface. (B) Image charge effects due to the chirality-dependent dielectric properties of the SWCNT core mitigate or enhance the effective electrostatic charge on each of the negatively charged phosphates along the ssDNA backbone. (C) vdW-Ld energy differences result from chirality-dependent optical properties.

All three of these options are equally plausible. They would, in fact, occur simultaneously because they are all coupled to geometry. Geometry determines the locations of the carbon atoms and how their bond angles twist, which influences option (A). Options (B) and (C) both depend on the optical properties and/or full electronic structure: both have a well known dependence on chirality/geometry. Despite the fact that options (A)–(C) are inherently coupled and cannot be isolated to study independently, it should be possible to determine which options have the greatest impact and whether they agree with the experimental results.

Manohar *et al.*¹⁵ studied option (A) by using classical force field computer simulations. They concluded that there is, in fact, a distinct energy dependence of a nucleotide as a function of position along the sp^2 lattice of the $[10,10,m]$ SWCNT. For a single nucleotide allowed to sample/slide along the entire SWCNT geometrical landscape, the maximum difference was found to be approximately 2 kT. This is a significant result, but it remains to be seen how much this per nucleotide energy changes when using multiple nucleotides in the same simulation. The latter will likely reduce this energy because it is impossible to have perfect coherence between the neighboring nucleotides to reside equally in the neighboring 2 kT energy wells. Bond stretching, bond twisting, and other effects would also have to occur and would result in additional energy penalties. More simulations are needed before a final determination can be made.

Option (B) was explored by Lustig *et al.*¹² The resulting Manning condensation model for ssDNA/SWCNT hybrids agreed exactly with the experimental outcome of Zheng *et al.*¹⁵ for the metallic versus semiconducting separation. However this extension to the Manning model was created when the separation was believed to be predominantly between metals and semiconducting tubes, which have a large theoretical difference in their direct current (DC), zero frequency electrostatic term (metals have a theoretical infinite polarizability at near 0 eV frequencies).¹² Later experiments by Zheng and Semke¹¹ have shown an ability to separate semiconducting tubes consistently and robustly. Of particular significance was the ability to separate the $[6,5,s]$ and $[9,1,s]$, which have theoretically identical band gaps and tube diameters. So while the effect of image charging [option (B)] is undoubtedly still present, it is probably less likely to explain the separation between semiconducting species. (The large differences in the dielectric constants are no longer present.) It is possible that option (A) (chirality-dependent surface charging) and option (B) (image charging) are work-

ing together. Option (B) could have an impact in the separation between the larger classes (metallic versus semiconducting); while option (A) allows for a more graded separation within a class (i.e., the $[6,5,s]$ versus $[9,1,s]$). These are still speculations that need to be tested/addressed and are well beyond the scope of this paper.

Lastly, option (C) (chirality-dependent vdW-Ld interactions) is what this paper and its predecessors explore. The two barriers to achieve this were the lack of full spectral optical properties for each SWCNT chirality and the lack of a Lifshitz formulation that could handle both the geometry and optical anisotropy of a SWCNT. Without optical properties for each SWCNT, it would be impossible to determine the relative differences among the various chiralities because all vdW-Ld interaction energies would be derived from the same approximated input (i.e., graphite or graphene). *Ab initio* calculations were used to obtain the optical information and clear differences were observed between SWCNT chiralities (i.e., the $[6,5,s]$ semiconductor and the $[9,3,m]$ metal) as well as between the independent directions of a single SWCNT (i.e., radial versus axial direction of a single tube). Initial Hamaker coefficients were crude comparisons between the axial-axial, axial-radial, and radial-radial interactions, but they made a strong case for orientation and chirality-dependent vdW-Ld properties.⁵ This was the catalyst for the derivation of the optically anisotropic solid-cylinder Lifshitz formulations that gave more realistic results as a function of the separation distance and orientation.⁸

The next step to explore option (C) further is to include spatially varying optical property effects in the analysis. This would allow one to calculate Hamaker coefficients and vdW-Ld interactions for systems and/or experiments that employ surfactants and large and small diameter SWCNTs and multiwalled carbon nanotubes (MWCNTs). The objective of this article is to create effective solid-cylinder spectra from realistic, multi-component SWCNT materials in order to achieve this end.

III. THEORY

Calculating Hamaker coefficients and total vdW-Ld energies is typically done by the Lifshitz formulation, which is a first principles quantum electrodynamic (QED) approach that takes into account all the multibody interactions and boundary conditions. The original derivation was for two semi-infinite half-spaces separated by an isotropic medium,¹⁶ but many different extensions have been added to allow for the inclusion of different geometries and optical anisotropies.¹⁷ We recently extended the vdW-Ld formulations to calculate Hamaker coefficients and total vdW-Ld energy interactions for two systems relevant for SWCNTs.⁸

- (a) Two optically anisotropic solid cylinders interacting with each other.
- (b) An optically anisotropic solid cylinder interacting with an optically anisotropic substrate.

For those wanting to understand the physical origins and many nuances of the Hamaker coefficients presented in this paper, we cannot emphasize enough the benefit of having the

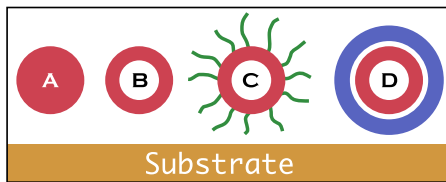


FIG. 1. (Color online) The many levels of interactions with a substrate. (a) A solid cylinder, (b) a hollow cylinder, (c) a hollow cylinder coated with a surfactant, and (d) a hollow cylinder within a cylinder.

two previous references at hand. Lifshitz formulations are often poorly understood and implemented for many historical reasons (many different notations used, lack of spectral data, inclusion of pairwise additivity, etc). However we also realize that these two references are quite involved and can be too much for casual readers interested in just knowing qualitative information. Therefore in order to strike a balance, we have included what we consider the most critical features of the original and anisotropic solid-cylinder formulations in Appendix A for a quick reference.

Figure 1 shows several systems of interest for experimentalists, ranging from a single solid cylinder to coated SWCNTs and MWCNTs. The systems can be made even more complex by using nonuniform surfactant coverage or nonconcentric MWCNTs, but we shall stick to the simpler cases in order to clearly illustrate a proper strategy. The major difference between these systems from a vdW-Ld standpoint is that the optical properties vary spatially as a function of radius. Understanding the radial dependence of the optical properties at the far-limit (surface-to-surface separation greater than two cylinder diameters) is necessary to calculate the total energy and the Hamaker coefficients, which respectively depend on the interacting volume size and optical properties contained within that volume. Ideally one would do this via an add-a-layer approach like the one used in plane-plane geometries, which can include an arbitrary quantity of layers of arbitrary thicknesses for each material.¹⁷⁻²¹ Unfortunately, analytically tractable add-a-layer solutions do not appear to be achievable within the cylindrical geometry systems at the moment.

Fortunately, there is the sensible alternative of using effective spectra in each limiting case (near/far limits) such that we can still use the solid-cylinder formulations without loss of realism, which is, of course, our chief concern when using any approximation. To be able to use the solid-cylinder formulations while not sacrificing accuracy, one essentially needs two primary inputs:

- (a) The optical properties of all the constituent materials present (medium+SWCNT+outer surfactant+core material).
- (b) A sensible spectral mixing formulation that can give us effective averaged optical spectra of the entire object.

Therefore we use spectral mixing at the far limit to determine the effective optical properties for the axial and radial directions.²²⁻²⁴ For all geometrical arrangements at the near limit (i.e., less than 0.5 nm surface-to-surface separation), the vdW-Ld properties of the surfaces on each material

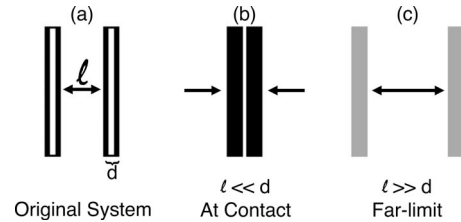


FIG. 2. The behavior of the overall effective optical properties on the Hamaker coefficient as a function of separation distance ℓ . (A) Original layered system with a thickness of $2a=d$. (B) At near contact ($\ell \ll a$) it is the optical properties near the respective surfaces that dominate the interaction. (C) At large separations ($\ell > 4a$), the optical properties are a weighted average of the various components and usually dominated by the materials with the larger volume fraction.

tend to dominate the interaction (Fig. 2) because of the divergent behavior of the total energy scaling. This is well known for plane-plane geometries.¹⁷ However, it is worth illustrating this point further because it is critical to our assertion that spectral mixing is viable and (if no analytical formulations exist) necessary at the far limit and not an acceptable practice at the near limit. This is also included in Appendix A.

A. Mixing rules for far-limit behavior

The study of vdW-Ld interactions for SWCNTs at the far limit is particularly exciting from an optical anisotropy standpoint because the $\Delta_{\parallel} = (\epsilon_{\parallel} - \epsilon_m) / \epsilon_m$ term within the Hamaker coefficient summation can go over unity when $\epsilon_{\parallel} \gg \epsilon_m$. Without this restriction, each Matsubara frequency in the Lifshitz summation can contribute to the overall direction-dependent vdW-Ld properties in a very significant way.^{8,17} In terms of spectral mixing considerations, we are no longer dealing with distances approaching contact and therefore must average the optical properties to get an effective solid cylinder. Typically, the spectral mixing of optical properties is done via an effective medium approximation (EMA), such as Bruggeman EMA.²⁴ The basic form is as follows:

$$\sum_i \phi_i \frac{\epsilon_i - \epsilon}{\epsilon_i + 2\epsilon} = 0, \quad (1)$$

where ϕ_i is the volume fraction of each component. From a physical standpoint, the unmodified Bruggeman EMA lacks any predominant geometrical arrangement of material connectivity in a particular direction. One can make a case that the radial direction of a SWCNT also lacks a predominant geometrical arrangement. If we slice a cross section and discretize it into small units, some parts would behave like a series capacitor and others (e.g., the circumferential portions within the cylindrical shell) would behave more like capacitors in parallel. Therefore using either of the end points (e.g., series or capacitor mixing) would not be a valid approach and the Bruggeman EMA appears to be the best balance.

In the axial direction, the polarization can easily be split into well defined regions of continuous connectivity. Therefore a cross sectional area weighing (i.e., a parallel capacitor averaging) is valid. This is particularly important for the metallic SWCNTs, which tend to have a very large (100+)

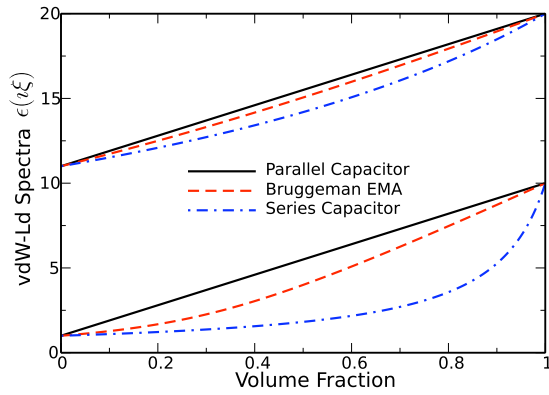


FIG. 3. (Color online) Comparison of the parallel capacitor, Bruggeman EMA, and series capacitor spectral mixing approximations. (a) Bottom 3 curves: When the magnitude of one spectrum is many times larger than the other (which is typical in the DC or 0 eV limit of metallic SWCNTs), the different models exhibit more variation as the connectivity becomes important. (b) Top 3 curves: When the optical spectra are similar in magnitude, all three models converge to similar values for any volume fraction, and therefore, the choice of which particular mixing formulation to use is less of an issue.

vdW-Ld spectra peak at 0 eV. If we used the EMA mixing rule, the axial direction spectra at 0 eV would be artificially lowered and the Δ_{\parallel} terms would not contribute as strongly to the overall total energy.

Figure 3 shows a comparison of the parallel capacitor, Bruggeman EMA, and series capacitor mixing formulations for two materials with varying volume fractions. When the optical properties of two materials at a given frequency are very close in magnitude, the variation among the three models is quite small. However, in the situations where there is a large difference, the parallel capacitor model evenly weights the two spectra by volume fraction, while the Bruggeman EMA is considerably damped by the weakest of the two or more spectra magnitudes. The series and parallel capacitor methods represent the limiting cases of connectivity, while the Bruggeman and other EMAs can be thought of as intermediate arrangements of the material connectivity in three dimensional space.

It should be noted that there are many other mixing formulations available, such as Lorentz–Lorenz, Maxwell–Garnett, and Rayleigh. However, the Lorentz–Lorenz assumes a vacuum host instead of any arbitrary medium or additional materials. This would be insufficient to create a MWCNT out of two or more SWCNT components. The Maxwell–Garnett assumes a dilute volume fraction within the host material. While the SWCNTs can certainly be diluted in the water medium, the mixing formulation itself is done within the confines of the other shell layer of the SWCNT. Therefore it really cannot be considered dilute from that perspective. The Rayleigh mixing tends to give far too much weight to the weaker of the two spectra, closely representing the effects of the series capacitor. Therefore it is also not an ideal candidate for SWCNTs.

The Bruggeman EMA mixing formulation tends to be the most appropriate for our SWCNT systems because it does not assume which material is the host (i.e., dominant or majority material) or assume a predominant connectivity. If such a situation did arise where one needed additional con-

TABLE I. A comparison of the effects of the different mixing formulations on a 50–50 mixture of the [25,0,*s*] radial direction and vacuum.

Mixing formulation	vdW-Ld (0 eV)	vdW-Ld (1 eV)	\mathcal{A}_{121}
Parallel capacitor	5.87	3.84	82.10
Perpendicular capacitor	1.83	1.74	29.84
Bruggeman EMA	4.21	3.02	63.90
Maxwell–Garnett	5.00	3.37	53.28
Lorentz–Lorenz	2.86	2.46	70.23
Rayleigh	2.42	2.17	44.92

nectivity in the radial direction, but not quite reaching the parallel limit, straightforward interpolations are available to achieve every gradation in between.²⁴ In short, the Bruggeman EMA can be interpolated to all of the other models with a simple q factor varying from 0 (zero screening parallel capacitor) to 1 (series capacitor). We use the traditional Bruggeman EMA for the purposes of this paper, but leave the door open for further refinements on this q factor if it is needed in certain situations.

To quantify the impact of the mixing formulations, Table I compares the effects of six different mixing rules on a 50–50 mixture of the [25,0,*s*] radial direction with vacuum. This particular SWCNT was chosen because it does not have a metallic 0 eV behavior and its core void space is exactly 50% of the total volume of the entire SWCNT+core. The parallel and series capacitor methods are still the end points, resulting in the largest and smallest possible magnitudes, respectively. The Maxwell–Garnett model resides between the EMA and parallel capacitor and the Lorentz–Lorenz and Rayleigh models are much closer to the series capacitor model. The variation between these different models is quite large. Both the Hamaker coefficients and the effective vdW-Ld spectra can vary by a factor of 3. Therefore, it is important to choose the model carefully for a given geometrical system, particularly for complex and multicomponent systems.

B. Obtaining optical properties

We use an orthogonal linear combination of atomic orbital *ab initio* optical property method^{25–29} to obtain the imaginary part of the dielectric spectrum over real frequencies $\epsilon''(\omega)$ for each SWCNT. This involves taking a single unit cell of SWCNT along the axial direction and placing it into an infinite periodic array. The resulting $\epsilon''(\omega)$ from 0 to 45 eV is a raw “bulk” spectrum averaged over the entire super cell volume. However, our SWCNTs are unlike most bulk crystal calculations in that they only occupy a fraction of this total volume. Therefore we need to scale the raw optical properties by a factor of the total super cell volume/SWCNT volume. If we use half of the graphite interlayer spacing as the excluded volume (i.e., $d_0/2 \approx 1.65$ Å in outward and inward directions), this scale factor for the “hollow-cylinder” SWCNT spectra would be

$$\frac{xy}{(r+d_0)^2 - (r-d_0)^2}. \quad (2)$$

Here x and y are the original dimensions of the *ab initio* super cell (ranging anywhere from 12 to 45 Å, depending on

the SWCNT/MWCNT radius). The radius r here is the one typically defined as the distance from the center of the SWCNT cylinder to distance of the carbon atom centers. We call the spectra that result from Eq. (2) as the hollow-cylinder spectra because we have scaled out the core volume in addition to the void space around the outer wall of the SWCNT. In short, we have confined the optical properties just to the SWCNT shell volume and nothing more (i.e., the properties of the core and/or surfactant are independent). If we did not scale out the center core, we would have the “solid-cylinder” spectra, which would obviously be smaller in magnitude because the optical properties are spread or averaged out over a larger volume. The clear advantage in working with hollow-cylinder spectra is that we can easily use the spectral mixing rules to add a vacuum or water layer within the core and go back to the solid-cylinder spectra quite easily. We are therefore unlimited in our ability to vary what we can calculate.

One last important point needs to be addressed before going through the results and discussion. The use of *ab initio* optical properties tends to draw a certain level of apprehension from many who only want to use experimental data for the purposes of optical properties. However, many of the fears are unfounded as the resulting spectra have compared very favorably to experimental systems. A good example is Al_2O_3 , in which the difference between the *ab initio* results and an experimentalists’ optical properties are on the order of that typically observed between the results of two different experimental setups.³⁰ However, *ab initio* codes do more than just agree with experimental results (although that in itself is very useful). The additional benefits and advantages of such a tool are as follows:

- The ability to calculate full spectral optical properties for nanoscale materials with complex geometries (difficult to do with reflectance/transmission experiments requiring smooth/flat surfaces);
- the ability to resolve optically anisotropic directions;
- the ability to calculate full spectral optical properties of liquids;
- the ability to calculate full spectral optical properties in a native environment (e.g., DNA in water) in order to capture the effects of relevant secondary bonding on the optical properties (experimental methods to obtain deep UV spectra typically need dry, mounted samples that results in distorted bond angles and removal of adsorbed species).
- the ability to resolve the optical spectra as a function of the spatial coordinates in three dimensions (important for proteins and other nonuniform entities);
- the ability to quickly catalog large quantities of materials (lack of optical spectra continues to plague those interested in calculating vdW-Ld properties); and
- increased accuracy for a larger frequency range only requires additional computational power (experimental equipment necessary to obtain a large enough frequency range of optical properties is somewhat inaccessible to a large population).

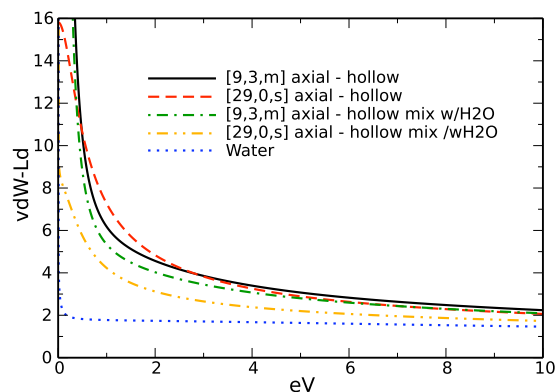


FIG. 4. (Color online) Here we see the hollow-cylinder and the hollow-cylinder spectra mixed w/ H_2O for the $[9,3,m]$ and $[29,0,s]$ SWCNTs in the axial direction. Note that the $[9,3,m]$ spectra only shift a little while the effect on the $[29,0,s]$ is much more dramatic because of its substantially larger core volume.

This is not to discount the value and desire for experimental data, which has proved to be tremendously useful in a variety of systems, particularly glasses and intergranular films. Rather the use of *ab initio* spectra simply opens the door to explore materials and systems that were previously unobtainable by means that are currently available. It should be seen as a useful and complimentary method and not as a replacement.

IV. RESULTS

Figure 4 shows the $[9,3,m]$ and $[29,0,s]$ SWCNT hollow-cylinder spectra and the resulting mixed w/ H_2O spectra in the axial direction using isotropic water uniformly distributed and filling 100% of each SWCNTs respective core. Of course, the core can be filled with any percentage of water from 0% to 100%. In this study, we assume a 100% of filling of isotropic order to have a standard benchmark across all tubes. If we were using the smallest of constructible nanotubes (e.g., the $[5,0,s]$), any water filling would not be possible as there is not enough void space to fit them within. A slightly larger diameter would allow for some water molecules but they would not have all rotational degrees of freedom and the assumption of the isotropic spectra would not hold. The tubes presented in this study are large enough that these issues should not arise.

Although there are many alternative water spectra by which to choose from,^{31–34} we use the index of refraction oscillator model by Parsegian¹⁷ because it accurately captures the zero frequency, matches index of refraction along the visible frequencies, and is easily recreated using simple damped oscillators. The other available models do make certain improvements (such as fulfilling the requirements of the f -sum rule,³⁴ etc.) and are equally valid for use. In general, the water spectrum is smaller in magnitude than the all SWCNT spectra for all frequencies. This has the effect of decreasing the overall magnitude of the effective, mixed w/ H_2O spectra in comparison to the hollow-cylinder spectra. The effect is clearly strong for the $[29,0,s]$, which is 55% hollow and therefore experiences a considerably shifting (the $[9,3,m]$, by comparison, is only 18% hollow). The implica-

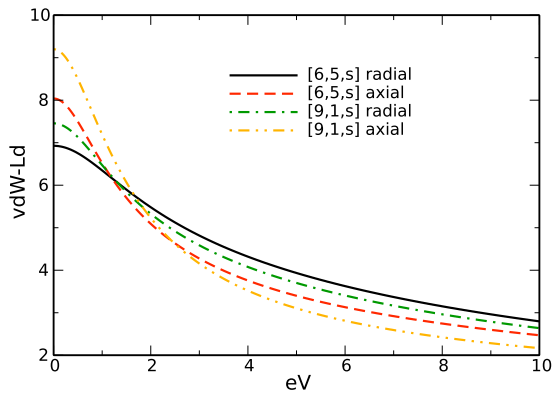


FIG. 5. (Color online) Here we see the hollow-cylinder spectra for the $[6,5,s]$ and $[9,1,s]$ SWCNTs in the axial and radial directions. The differences that exist are enough to cause a 5% change in the relative Hamaker coefficient strengths.

tions of this dampening show up clearly in the Hamaker coefficient calculations between the various chiralities (Table III). However, effects such as alignment and torque forces may increase or decrease depending on the relative positioning on the initial and final vdW-Ld spectra with that of the medium. In the particular examples found in this paper, they all diminish as well.

Figure 5 shows the comparison of the $[6,5,s]$ and $[9,1,s]$ axial spectra in both the hollow and mixed with water forms. Although the $[9,1,s]$ has a larger low energy wing, the $[6,5,s]$ has spectra that are larger in magnitude for the remainder of energy range. It is important not to neglect this small but important difference because the spectral mismatch terms contained in the Lifshitz formulation can still contribute to a very large energy range (e.g., 50+ eV). Moreover, even if an individual contribution at a given Matsubara frequency is not large all by itself, a lot of these terms put together can and do have noticeable effects. Table II lists the resulting energies for these two SWCNTs interacting with a polystyrene substrate across water. The polystyrene spectrum was obtained experimentally³⁵ and is publicly available.²¹ In each limit, the $[6,5,s]$ has the stronger Hamaker coefficient and thus has a stronger attraction. This result agrees with the experimental results of Zheng and Semke.¹¹ This agreement is encouraging because it suggests that the vdW-Ld terms agree with the overall effect. It remains to be seen how well additional results will compare to the elution experiments as well as the separation experiments by dielectrophoresis.¹³

TABLE II. The Hamaker coefficients for the optically anisotropic cylinder-water-polystyrene substrate system for the $[9,1,s]$ and $[6,5,s]$ SWCNTs in the near (hollow-cylinder spectra) and far (mixed w/H₂O spectra) limits. Values of $\mathcal{A}^{(2)}$ are all 0 because bulk amorphous polystyrene is isotropic and therefore there is no angular dependency.

SWCNT	Limit	Spectra type	$\mathcal{A}^{(0)}$ (zJ)
$[6,5,s]$	Near	Hollow	29.4
$[6,5,s]$	Far	Mixed w/H ₂ O	29.0
$[9,1,s]$	Near	Hollow	27.4
$[9,1,s]$	Far	Mixed w/H ₂ O	27.2

In Appendix B, we illustrate an example using fictitious spectra created from using simple damped oscillators to show how the mixed and unmixed cases converge to nearly the same total energy in the far limit. This demonstration using a fictitious system is convincing in and of itself. It would be even more convincing to use an actual system that contains both the component and total target vdW-Ld spectra. In particular, we would like to check two assumptions: (A) that the neighboring materials exhibit little or no coupling and/or alteration of each other's optical properties and (B) that the mixing formulations we chose for the radial and axial directions can, in fact, take constituent vdW-Ld spectra and accurately recreate a total vdW-Ld spectra.

Fortunately, a comparison of MWCNT and SWCNT spectra affords just such an opportunity to check both assumptions. Figure 6 shows the raw unscaled ϵ'' data for the $[16,0,s+7,0,s]$ MWCNT in comparison to the raw unscaled spectra of the constituent $[16,0,s]$ and $[7,0,s]$ SWCNTs. Clearly, the major trends are exactly additive. In the radial direction, the predominant discrepancies arise within the 10–20 eV range and are most likely the result of the out-of plane stacking effects between the two graphene-like layers. In the axial direction, there are small but relevant shifts in the first van Hove singularities occurring between 0 and 5 eV. The distance between the radii of the $[16,0,s]$ and $[7,0,s]$ SWCNT shells for a symmetrically arranged MWCNT is theoretically 3.523 Å and is thus only 0.2 Å larger than the equilibrium layer spacing in graphite. So we are reasonably confident that there is some coupling of the neighboring layers, but that this effect will not get much stronger than what is presently observed. It remains to be seen whether or not the electronic conduction properties in the axial direction can be switched from semiconducting to metallic or vice versa because of this interaction. We do not expect this to be the case, although some reported theoretical examples in which large transverse electric fields can shift the electronic bands and turn metallic CNTs into semiconducting.^{36–39}

The next assumption to test is the accuracy of the mixing rules, keeping in mind the effects of the nonlinear coupling. Figure 7 shows the vdW-Ld spectra for a $[16,0,s+7,0,s]$ MWCNT, a MWCNT created by mixing the $[16,0,s]$ and $[7,0,s]$ SWCNTs and the two SWCNT spectra. In both the axial and radial directions, the optical properties of the SWCNT constituents are quite different from those of the MWCNT. However, we obtain a very good approximation when we mix them via the combined parallel capacitor and Bruggeman mixing formulation described earlier. Note the excellent agreement in the axial direction with only a slight discrepancy of 8% at the 0 frequency term (which quickly drops to 2% difference for frequencies beyond 1 eV). The discrepancy in the radial direction is approximately 5%–6% over most of the frequency range.

Determining the physical origin of any resulting discrepancies is important so we do not compensate in such a way that might be improper or more problematic in the future for other systems. There are essentially three possibilities to address: (1) we chose the wrong mixing formulation, (2) improper scaling of the raw spectra into the hollow-cylinder

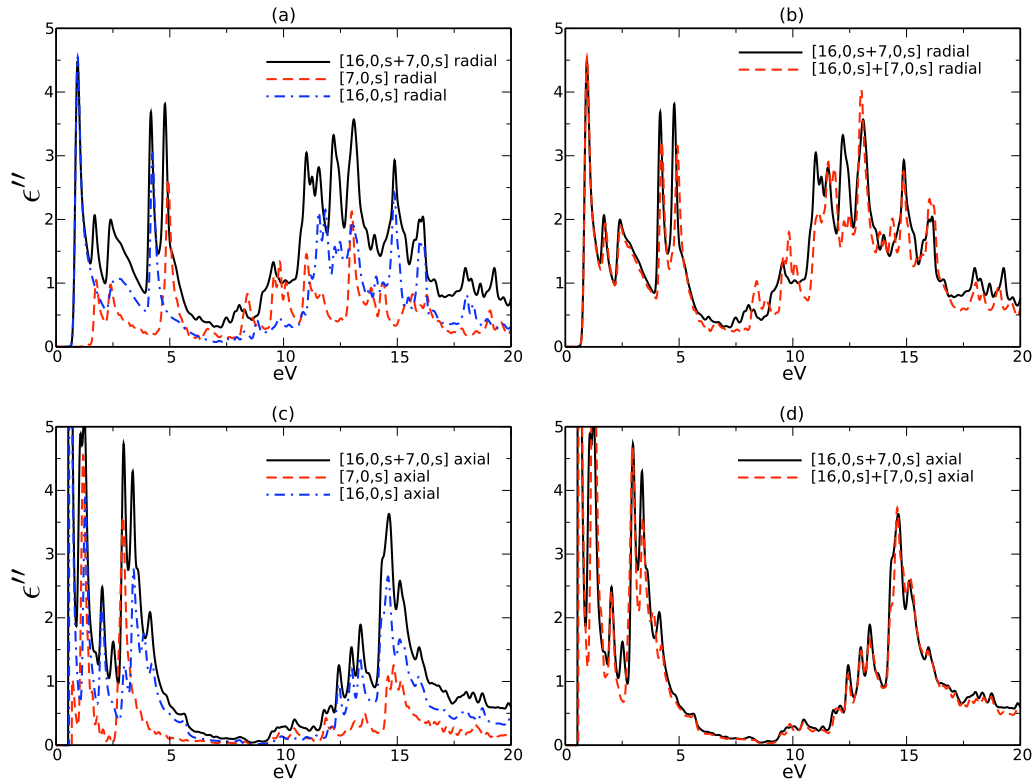


FIG. 6. (Color online) Compared the unscaled $[16,0,s+7,0,s]$ MWCNT ϵ'' data with the raw unscaled $[16,0,s]$ and $[7,0,s]$ SWCNT data for the radial and axial directions.

spectra for either the SWCNT or the MWCNT, and/or (3) nonlinear coupling effects existing between the neighboring layers. If our choice of mixing formulation was the problem, then simply going from a Bruggeman EMA mixing in the radial direction to a parallel capacitor method would give us the needed boost to match the stronger vdW-Ld of the calculated MWCNT. However, if we look closely at the 0–1 eV range in the radial direction spectra in Fig. 7, the magnitudes of both constituent SWCNT spectra are below that of the MWCNT. Resolving this difference by changing the mixing rule is therefore impossible because the output values of all three mixing formulations are bound within the magnitude range of their pure constituents.

Perhaps the choice of scale factors is incorrect. If we were to increase the thickness of our SWCNT cylinder

boundary layers such that the inner and outer shells of our MWCNT overlapped, then we could easily make the case for reducing the MWCNTs overall scale factor by approximately 3%. As it is, we specifically chose the $[16,0,s+7,0,s]$ MWCNT because its equilibrium spacing between the shells is 0.2 \AA greater than the equilibrium spacing for graphite. So while this certainly gives us the change we would want, it really depends on whether picking or assuming this larger thickness is in reality a physically appropriate change.

The third and most likely reason for this difference is some of the coupling that occurs between the neighboring layers that affects the underlying optical properties of each layer present. Observing Fig. 6, we can see that for the majority of the spectra the MWCNT behaves very much like a simple addition of the two SWCNT spectra. There are, how-

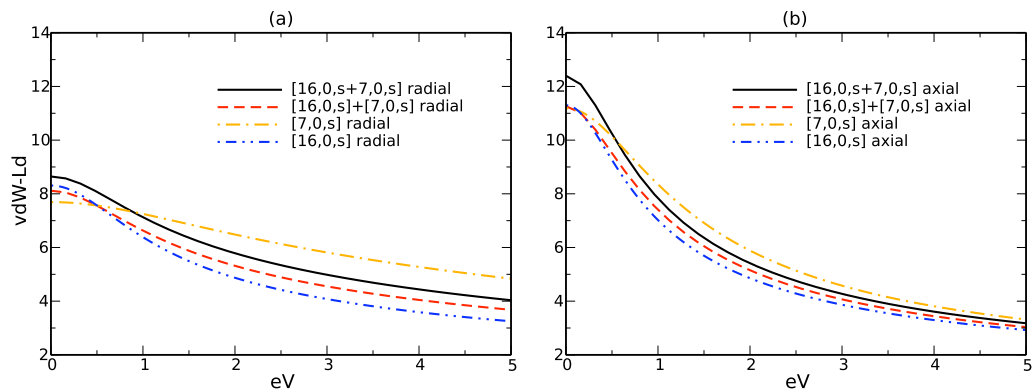


FIG. 7. (Color online) Compared the hollow-core MWCNT $[16,0,s+7,0,s]$ vdW-Ld spectra vs the effective MWCNT spectra created by mixing the $[16,0,s]$ and $[7,0,s]$ hollow-cylinder spectrum constituents.

TABLE III. Calculated cylinder-cylinder Hamaker coefficients ($\mathcal{A}^{(0)}, \mathcal{A}^{(2)}$) for the $[6,5,s]$ and $[9,3,m]$ SWCNTs using the raw optical properties scaled to a solid cylinder, scaled to a hollow cylinder, and a hollow cylinder mixed with a water core. The solid and mixed w/H₂O spectra are equally valid at the far limit depending on whether the core is filled with vacuum or water.

		Near-limit $\mathcal{A}^{(0)}, \mathcal{A}^{(2)}$ (zJ)			Far-limit $\mathcal{A}^{(0)}, \mathcal{A}^{(2)}$ (zJ)		
n	m	Solid	Hollow	Mixed w/H ₂ O	Solid	Hollow	Mixed w/H ₂ O
9	3	62.3, 0.5	91.7, 0.6	66.7, 0.5	107.0, 36.2	163.3, 56.6	113.3, 36.8
6	5	85.0, 0.1	111.8, 0.1	88.0, 0.1	105.6, 1.9	144.2, 3.3	110.5, 2.2
9	1	72.3, 0.4	95.6, 0.4	75.3, 0.3	92.8, 3.0	126.9, 4.9	97.4, 3.3
29	0	14.3, 0.0	71.8, 0.1	20.1, 0.1	18.5, 0.8	108.6, 8.6	26.2, 1.3
Valid		N	Y	N	Y	N	Y

ever, small areas where the calculated MWCNT has stronger transitions. These significantly add to the overall vdW-Ld spectra and give it its increased magnitude over spectra created from SWCNT.

In light of these minor discrepancies, a valid question to ask is why one would ever use SWCNT spectra to create MWCNT spectra instead of just obtaining the MWCNT properties directly. Their are a couple of key answers. First, it eliminates much of the sheer computational difficulty that it would take to obtain the properties of certain MWCNTs and other multicomponent systems. For example, suppose we want to create a MWCNT that has almost an exact graphite interlayer spacing separation between the two rings, an ideal choice with this separation distance would be the $[10,10,m]$ and $[6,4,s]$. However, the ratio of their cell heights for the *ab initio* calculation is not commensurate and would require 11 repeat units of the $[6,4,s]$ and 83 of the $[10,10,m]$ in order to come close to synchronizing up. This would require 4992 atoms—not an impossible number but certainly one to two orders of magnitude larger than most SWCNTs. Moreover, this is the low end, as it is possible to mix two SWCNTs together that might require even more atoms than this or require some form of stretching/distortion along the backbone in order to minimize this effect. Going to three-ring or four-ring MWCNTs would exacerbate this problem even further.

There is a second and equally important reason to use SWCNT components even if obtaining a particular MWCNT spectrum was feasible. As explained in the analysis of Eq. (B6) for the cases C1/C2/C3 in Fig. 9 (see Appendix B), it is the optical properties of the two closest interfaces across the separation medium that dominate the total vdW-Ld interaction energy at distances near contact. The total MWCNT spectrum is, in fact, an averaged set of optical properties in the radial and axial directions and would not be valid at the near limit. By using the SWCNT pieces, we now can spatially resolve the optical properties in the way necessary to get the proper near-limit interaction. This effect would be the most important and influential when the different layers in a MWCNT contained both metallic and semiconducting species. Driving the point further, two MWCNTs might have very similar total vdW-Ld spectra but differ greatly in their outer shell properties.

So far we have described the importance of using the properly scaled and mixed spectra at the proper surface-to-

surface separation limit. However, now we want to demonstrate quantitatively the effects of each combination of scaling and mixing (solid, hollow, and hollow mixed w/H₂O) at each limit to show that the differences are very noticeable. Table III lists the calculated values of $\mathcal{A}^{(0)}, \mathcal{A}^{(2)}$ in zJ for the $[9,3,m]$, $[6,5,s]$, $[9,1,s]$, and $[29,0,s]$ using all three spectra varieties in the near and far limits of the optically anisotropic cylinder-cylinder systems.

Our initial values for the $[6,5,s]$ and $[9,3,m]$ across water are identical to the values we calculated and reported using the solid-cylinder optical properties.⁸ When we scale the optical properties to that of the hollow-cylinder spectra, the magnitudes become much larger. It should be noted though that this enlargement at the near limit is not unreasonable. In fact, it brings the Hamaker coefficient magnitudes into closer agreement with those previously published for the anisotropic graphite vdW-Ld spectra in water.^{5,40} This is a direct result of the hollow-cylinder scaling in which the optical properties are properly confined into the SWCNT shell, which dominates the interaction.

Conversely, the Hamaker coefficients calculated from the hollow-cylinder spectra would be incorrect to be used for a total energy calculation in the far limit. They ignore the interactions of the SWCNT cores, which would likely be different and possibly repulsive depending on the nature of the other materials present. However, we can obtain an accurate total Hamaker coefficient and total interaction energy if we mix the hollow-cylinder spectra with whatever material that makes sense for the particular experimental system. In this analysis, we chose a 100% fill of isotropic water. The resulting mixed Hamaker coefficients in the far limit are smaller than the hollow-cylinder spectra and slightly larger than that of the original solid-cylinder properties. These relative rankings are completely logical and expected as the hollow-cylinder scaling assumes a core material optically equivalent to the outer shell, the solid-cylinder scaling assumes a zero or vacuum core, and the mixed with water spectra uses a core material that has an optical spectra that is closer in magnitude to vacuum than the SWCNT.

With respect to all the coefficients listed in Table III, we cannot stress enough that only certain combinations are actually realistic despite the ease of which we can calculate these values for any combination of system, distance limit,

and spectra scaling/mixing. To avoid any confusion, we specifically note in the final row which are valid combinations to be used.

V. DISCUSSION

Although scaling and mixing seem fairly simple, they are clearly important to keep in mind at different distance limits and for different SWCNT sizes. At the near limit, we can clearly see that changing from the solid to hollow-cylinder spectra can result in a substantial boost in the magnitude of the Hamaker coefficient by 20%–50%, for even the small diameter SWCNTs. This effect is even stronger as the tube diameter increases and the difference between the hollow and solid-cylinder spectra widens. For example, the $[29, 0, s]$ Hamaker coefficients vary by a factor of five to ten times when changing between the hollow and solid-cylinder scaling behavior. Therefore, it is critical to use hollow-cylinder spectra at near contact separations where the closest materials dominate.

The opposite is true in the far limit. Here the optical properties must be averaged over the entire cylindrical container because the overall vdW-Ld interaction is a result of the potentially competing interactions of all the constituents. Large diameter SWCNTs (e.g., $[29, 0, s]$) will then have an optical response that is highly damped by either the vacuum or water core. One might expect that the overall vdW-Ld total energy would be weaker because of a smaller Hamaker coefficient. However, the total energy for the SWCNT + water core system can still strengthen because of the radius to the fourth power dependence on the vdW-Ld interaction energy in the farlimit [see Eq. (A12) in Appendix A].

As the size of the interacting objects increases, the total vdW-Ld energy at a given surface-to-surface separation should also grow because there is more volume interacting. The Hamaker coefficient is primarily determined by the optical properties and essentially gives the per unit volume component of the total vdW-Ld energy interaction. Mixing of a SWCNT spectrum with water clearly dampens the magnitude of the overall Hamaker coefficients due to reduction in optical contrast. However, the volume of interacting substance can more than make up for this effect. For example, if we take far-limit hollow mixed w/H₂O values from Table III, the Hamaker coefficient or vdW-Ld interaction energy density of the $[6, 5, s]$ is four times greater than the $[29, 0, s]$. However, when we multiply by a^4 , the total interaction energy of two $[29, 0, s]$ interacting across a surface-to-surface separation ℓ is 20 times stronger. Therefore these contrary tendencies are important to keep in mind when making final determinations of what should happen in a given experimental procedure.

What then are the effects of surfactants? Although we did not specifically include surfactant coated SWCNTs in this paper, there is no additional conceptual difficulty from a computation or from a calculation standpoint. For example, a MWCNT with a water core and a uniform layer of sodium dodecyl sulfate (SDS, a typical SWCNT surfactant) would simply behave as a cross sectional area weighted mixing of the constituent spectra in the far limit and of pure SDS at the

near limit. One could then use the interpolation style suggested previously to obtain a vdW-Ld energy at all distances.⁸

The biggest limiting step preventing us from including surfactant effects is, as described earlier, the lack of optical spectra for all potential surfactant candidates over an energy range sufficient for the Lifshitz formulations. We are actively working to alleviate this after we finish publications on additional SWCNT spectra classifications. However, until robust spectral data are available, we are unable to carry this analysis any further other than describing qualitative trends that can occur. At the near limit, the ability to spatially resolve the SDS layer from the SWCNT or MWCNT is important for the same reason as described above when spatially resolving the SWCNT constituents from the bulk MWCNT optical property.

Experimental methods that determine bulk spectral properties of ssDNA/SWCNT hybrids and similar nanostructures would be pertinent for the far limit only. The near limit requires a spatial resolution and possibly directionally dependent properties, both of which are either impossible or extremely difficult to obtain experimentally for these types of systems. This further underscores the utility of *ab initio* methods as a viable and powerful alternative to obtain this information. Additionally, it underscores the need to catalog even the most basic of materials. Currently the only organic materials we have publicly available (outside of the carbon based SWCNTs) are polystyrene, tetradecane, and possibly a few others.^{35,41} With a larger database of SWCNTs and surfactant spectra, one can start data mining to find combinations favorable for one type of interaction over another.

Although the focus of this paper is SWCNTs, the solid-cylinder formulations can be used for any liquid crystal, protein, collagen, or any material in which the overall shape can be described as cylindrical. As long as one has the optical properties, one can obtain the per unit length or total energy of interaction for any of these systems. One can use the mixing rule analysis of Sec. IV for other geometries. For example, the vdW-Ld interactions of surfactant coated colloids could also be optically mixed with the Bruggeman EMA for the far limit. The overall themes described here for SWCNTs would be equally applicable to other systems.

VI. CONCLUSIONS

We have introduced spectral mixing rules to consider interactions composed of multiple layers varying in the radial direction. We create an effective set of homogeneous, anisotropic solid-cylinder optical properties from the original hollow-cylinder constituents. Our results show that the spectral mixing via a combination of a parallel capacitor rule in the axial direction and the Bruggeman EMA in the radial direction can result in reasonable vdW-Ld spectra, Hamaker coefficients, and total vdW-Ld behavior. Additionally, we have shown that there is some secondary bonding/coupling between the ϵ'' absorption properties of two SWCNTs with the resulting MWCNT. This feature warrants further exploration/investigation but it is presently considered here to be small enough for our assumption of independent layers

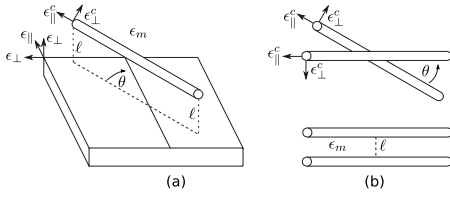


FIG. 8. The two systems that are now solvable by explicit analytical Lifshitz formulations in the near and far limits. (a) An optically anisotropic solid cylinder with an optically anisotropic substrate with its primary uniaxial polarization contained within the surface plane and (b) an optically anisotropic solid cylinder with another optically anisotropic solid cylinder.

to hold. Although the primary purpose of this paper is to give us the ability to calculate accurate Hamaker coefficients and total vdW-Ld energies of complex SWCNTs system (e.g., surfactants, SWCNTs mixed w/core materials, MWCNTs), the strategy presented here is widely applicable to other nanoscale/biological systems for which analytical add-a-layer Lifshitz formulations are not currently available.

ACKNOWLEDGMENTS

R. Rajter would like to acknowledge financial support for this work by the NSF under Contract No. CMS-0609050 (NIRT). R. Podgornik would like to acknowledge partial financial support for this work by the European Commission under Contract No. NMP3-CT-2005-013862 (INCENS). W. Y. Ching is supported by DOE under Grant No. DE-FG02-84DR45170.

This study was supported by the Intramural Research Program of the NIH, Eunice Kennedy Shriver National Institute of Child Health and Human Development.

APPENDIX A: KEY FEATURES AND CONCEPTS FOR THE OPTICALLY ANISOTROPIC ROD-ROD AND ROD-SURFACE LIFSHITZ FORMULATIONS

We recently extended the Lifshitz formulations to include the following systems in both the near and far limits.

- (a) Two optically anisotropic solid cylinders interacting with each other.
- (b) An optically anisotropic solid cylinder interacting with an optically anisotropic substrate.

Figure 8 shows these systems visually with the proper parallel and perpendicular optical directions clearly labeled. Both these systems have unique formulations for their respective near- and far-limit formulations, which we then originally applied to the $[6,5,s]$ and $[9,3,m]$ SWCNTs using the solid-cylinder spectra. In this analysis, we determined that the system is considered to be in the “far limit” regime when at a surface-to-surface separation distance “ l ” is approximately two full SWCNT diameters. The “near limit” is essentially contact and everything in between requires interpolation. The scaling law analysis used to make this regime limit the determination, as well as the complete derivation of the total solid-cylinder Lifshitz formulations, can be found in the original paper.⁸

For systems containing optical anisotropy, there exists the potential and opportunity for orientation-dependent

vdW-Ld energies and Hamaker coefficients. So rather than just having \mathcal{A} as a single Hamaker coefficient, it is split into two parts. The $\mathcal{A}^{(0)}$ is the Hamaker coefficient when the two ϵ_{\parallel} optical directions are 90° out of phase (see Fig. 8 again for a proper frame of reference). The $\mathcal{A}^{(2)}$ term is the additional Hamaker coefficient component when going from the 90° out of phase orientation to that of perfect (optical) alignment with the principal axis of the other object. Clearly, if there is no orientational preference, $\mathcal{A}^{(2)}$ goes to zero and we are back to a single Hamaker coefficient.

The cylinder-substrate and cylinder-cylinder formulations in both the near and far limits have the same overall structure for the Hamaker coefficient calculation, which is as follows:

$$\mathcal{A}^{(0)} = \frac{3k_B T}{2} \frac{1}{2\pi} \sum_{n=0}^{\infty} \int_0^{360} \Delta_{\mathcal{L}m}(\phi) \Delta_{\mathcal{R}m}(\phi - 90) d\phi, \quad (\text{A1})$$

$$\mathcal{A}^{(0)} + \mathcal{A}^{(2)} = \frac{3k_B T}{2} \frac{1}{2\pi} \sum_{n=0}^{\infty} \int_0^{360} \Delta_{\mathcal{L}m}(\phi) \Delta_{\mathcal{R}m}(\phi) d\phi, \quad (\text{A2})$$

where k_B is the Boltzmann constant. $\Delta_{\mathcal{L}m}$ and $\Delta_{\mathcal{R}m}$ are the spectral mismatch or spectral contrast functions of left and right materials across the neighboring medium. The integration occurs over all 360° within the plane perpendicular to the stacking direction. The summation in the expression above is not continuous but rather over a discrete set of Matsubara frequencies, $\xi_n = \frac{2\pi k_B T n}{h}$.^{16–18} The form of the Δ spectral contrast functions vary with the particular system we are dealing with. They are as follows for the near-limit anisotropic solid cylinder—anisotropic solid cylinder and near-limit anisotropic solid cylinder—anisotropic substrate systems:⁸

$$\Delta_{\mathcal{L}m}(\phi) = \left[\frac{\epsilon_{\perp}(\mathcal{L}) \sqrt{1 + \gamma(\mathcal{L}) \cos^2 \phi} - \epsilon_m}{\epsilon_{\perp}(\mathcal{L}) \sqrt{1 + \gamma(\mathcal{L}) \cos^2 \phi} + \epsilon_m} \right], \quad (\text{A3})$$

$$\Delta_{\mathcal{R}m}(\phi) = \left[\frac{\epsilon_{\perp}(\mathcal{R}) \sqrt{1 + \gamma(\mathcal{R}) \cos^2 \phi} - \epsilon_m}{\epsilon_{\perp}(\mathcal{R}) \sqrt{1 + \gamma(\mathcal{R}) \cos^2 \phi} + \epsilon_m} \right], \quad (\text{A4})$$

$$\Delta_{\mathcal{R}m}(\phi - 90) = \left[\frac{\epsilon_{\perp}(\mathcal{R}) \sqrt{1 + \gamma(\mathcal{R}) \sin^2 \phi} - \epsilon_m}{\epsilon_{\perp}(\mathcal{R}) \sqrt{1 + \gamma(\mathcal{R}) \sin^2 \phi} + \epsilon_m} \right]. \quad (\text{A5})$$

We drop the explicit (ξ) dependence for all ϵ materials and directions in order to keep the notation more legible, but it is always understood that these properties are a function of frequency. The γ term is a measure of the optical anisotropy for the left or right half-spaces in the near limit and has the form

$$\gamma = \frac{\epsilon_{\parallel} - \epsilon_{\perp}}{\epsilon_{\perp}} \quad (\text{A6})$$

The far-limit equations have a very different form because we could no longer use the Derjaguin approximation.¹⁷

For the far-limit optically anisotropic solid-cylinder—optically anisotropic solid-cylinder system, the spectral contrast terms are of the following form:

$$\Delta_{\mathcal{L}m}(\phi) = -\left\{\Delta_{\perp}(\mathcal{L}) + \frac{1}{4}[\Delta_{\parallel}(\mathcal{L}) - 2\Delta_{\perp}(\mathcal{L})]\cos^2\phi\right\}, \quad (\text{A7})$$

$$\Delta_{\mathcal{R}m}(\phi) = -\left\{\Delta_{\perp}(\mathcal{R}) + \frac{1}{4}[\Delta_{\parallel}(\mathcal{R}) - 2\Delta_{\perp}(\mathcal{R})]\cos^2\phi\right\}, \quad (\text{A8})$$

$$\Delta_{\mathcal{R}m}(\phi - 90) = -\left\{\Delta_{\perp}(\mathcal{R}) + \frac{1}{4}[\Delta_{\parallel}(\mathcal{R}) - 2\Delta_{\perp}(\mathcal{R})]\sin^2\phi\right\}, \quad (\text{A9})$$

where Δ_{\parallel} and Δ_{\perp} are as follows:

$$\Delta_{\parallel} = \frac{\epsilon_{\parallel} - \epsilon_m}{\epsilon_m} \Delta_{\perp} = \frac{\epsilon_{\perp} - \epsilon_m}{\epsilon_{\perp} + \epsilon_m}. \quad (\text{A10})$$

The values of $\mathcal{A}^{(0)}$ and $\mathcal{A}^{(2)}$ are obtained in a straightforward manner. One uses the Δ forms for the particular geometry and distance limit and adds in the spectra properties as the primary input. At this stage, we have the Hamaker coefficients but not the total vdW-Ld energy. To obtain that, one must then use vdW-LD energy scaling law behavior for the particular system, which also depends heavily on the geometry and distance limit of the system. For the far-limit solid cylinders at an arbitrary angle, the total vdW-Ld energy varies as follows:

$$G(\ell, \theta) = -\frac{(\pi a^2)^2 (\mathcal{A}^{(0)} + \mathcal{A}^{(2)} \cos^2 \theta)}{2\pi \ell^4 \sin \theta}, \quad (\text{A11})$$

where the two rods are assumed to be of equal radius a for this case. If we go to perfect alignment, the total energy for two infinitely long cylinders diverges. Therefore it is more relevant to report the energy per unit length as we derived previously,

$$g(\ell, \theta=0) = -\frac{3(\pi a^2)^2 (\mathcal{A}^{(0)} + \mathcal{A}^{(2)})}{8\pi \ell^5}. \quad (\text{A12})$$

In the near limit under perfect alignment, the two solid cylinders exhibit a much different, per length energy scaling law with distance,

$$g(\ell, \theta; a) = -\frac{\sqrt{a}}{24\ell^{3/2}} (\mathcal{A}^{(0)} + \mathcal{A}^{(2)}). \quad (\text{A13})$$

For the purposes of this paper, we are mainly interested on how the Hamaker coefficients are affected by mixing rules of the constituent optical properties and will therefore calculate many total vdW-Ld energies. Those interested can easily use the above equations with the reported Hamaker coefficients to graph and compare between the various SWCNTs.

The primary benefit of the anisotropic solid-cylinder formulations was the ability to quantify the relative strengths in Hamaker coefficients for each SWCNT chirality and to determine the vdW-Ld torques that arise from the morphological and optical anisotropies. Before these formulations existed, we had to use a crude pairwise comparison in order to show this effect qualitatively. That is, we took the radial and axial spectral components and created isotropic planar half-

spaces out of them to compare the differences between the radial-radial, radial-axial, and axial-axial components to see if there was a preferred interaction. For the $[9,3,m]$, there was clearly a major gain by maximizing the axial-axial interaction, making the case for alignment. While one can get away with doing this type of comparison for simple systems to get a rough approximation, it can lead to errors and incorrect predictions if one is not careful. The Lifshitz formulations are coupled with respect to the boundary conditions of all optical independent directions (see the derivation in Ref. 17 for additional information) and can result in values that are smaller, larger, or even opposite in sign to what one expects for complex systems.

Although the formulations are a much needed improvement, one must also be aware of certain aspects and assumptions contained within them and not blindly use them in a black box fashion. In particular, one important assumption contained within the present formulation is that the optical properties of the SWCNTs were visibly interacting like a spatially homogenous solid cylinder, which lacks any significant optical spectral contrast along the radial direction. This may be unimportant for very small diameter SWCNTs that lack a surfactant layer, but the spectral variation along the radial direction becomes very important for large diameter SWCNTs (e.g., a $[24,24,m]$ SWCNT is 67% hollow), MWCNTs, or any nanotubes covered with a surfactant layer of an appreciable thickness. This is why the mixing formulation considerations are so important in terms of creating effective spectra that can use these formulations and obtaining meaningful and accurate results.

APPENDIX B: TOTAL VDW-LD ENERGY EQUIVALENCE AT THE FAR LIMIT

Figure 9 details the concepts of Fig. 2 in a more rigorous quantitative fashion by comparing the total vdW-Ld energy ratios as a function of ℓ/a . For simplicity, we calculated the Hamaker coefficient using fictitious vdW-Ld input spectra by using simple damped oscillators of the following form:

$$\epsilon(\ell\xi) = 1 + \frac{s}{1 + \xi^2}, \quad (\text{B1})$$

where s represents the magnitude or strength of the oscillator. For Fig. 9, we chose a large value of $s=100$ for the unmixed solid material in case C3 and a value of $s=0$ for the vacuum. For the mixture material, we used the Bruggeman EMA at each Matsubara frequency (the details of the EMA mixing formulation will be described more rigorously in the next section). The total energy and Hamaker coefficients were calculated using the following simple nonretarded isotropic plane-plane equations:

$$\mathcal{G}(\ell) = \frac{\mathcal{A}}{12\pi\ell^2}, \quad (\text{B2})$$

$$\mathcal{A}_{\mathcal{L}m_1/\mathcal{R}m_2} = \frac{3}{2} \sum_{n=0}^{\infty} \left(\frac{\epsilon_{\mathcal{L}} - \epsilon_{m_1}}{\epsilon_{\mathcal{L}} + \epsilon_{m_1}} \right) \left(\frac{\epsilon_{\mathcal{R}} - \epsilon_{m_2}}{\epsilon_{\mathcal{R}} + \epsilon_{m_2}} \right). \quad (\text{B3})$$

Cases C2 and C3 required a slightly more complicated add-a-layer form of the overall energy. We use the following

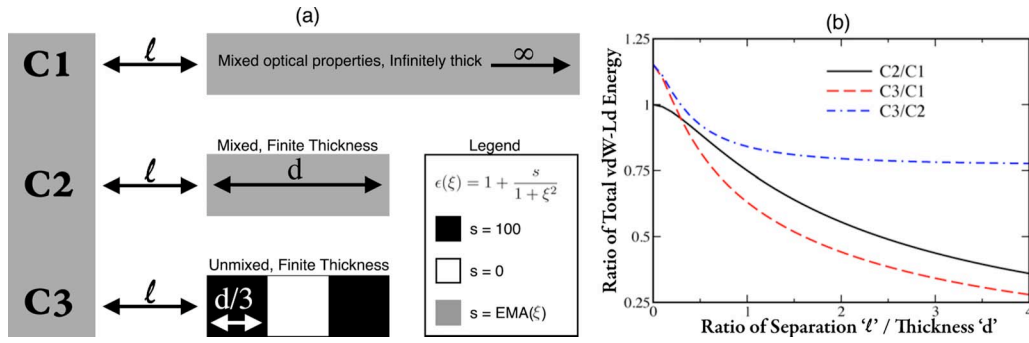


FIG. 9. (Color online) Compared total vdW-Ld interaction energy ratios of three different systems to demonstrate the utility of mixing formulations in the far limit. (A) Case C1 uses the optically mixed material in an infinitely thick configuration. Case C2 is a finite block of the optically mixed material. Case C3 contains the unmixed material sandwiching a vacuum layer. (B) The ratio of total vdW-Ld energies varies as a function of the dimensionless scale factor l/a .

(see Ref. 17) subscript notation, i.e., $\mathcal{A}_{\mathcal{L}m/\mathcal{R}m}$, so as to eliminate confusion. Here the slash in the subscript denotes the sides to the left and right of the medium. The first term in each subscript couple denotes the material farthest away from the middle/intervening separation layers. If we label the EMA mixture material as m , the low value vacuum as v , and the high value of the solid material as h , then the cases C1, C2, and C3 would be solved as follows:

$$C1: \mathcal{G}(\ell) = \frac{-\mathcal{A}_{mv/mv}}{12\pi(\ell)^2}, \quad (B4)$$

$$C2: \mathcal{G}(\ell) = \frac{-\mathcal{A}_{mv/mv}}{12\pi(\ell)^2} + \frac{-\mathcal{A}_{mv/vm}}{12\pi(\ell+a)^2}, \quad (B5)$$

$$C3: \mathcal{G}(\ell) = \frac{-\mathcal{A}_{mv/hv}}{12\pi(\ell)^2} + \frac{-\mathcal{A}_{mv/hv}}{12\pi(\ell+a/3)^2} + \frac{-\mathcal{A}_{mv/hv}}{12\pi(\ell+2a/3)^2} + \frac{-\mathcal{A}_{mv/hv}}{12\pi(\ell+3a/3)^2}, \quad (B6)$$

Equation (B6) may look bulky but there is a clear and easy to understand pattern that arises when moving from C1 to C3. In short, the total energy equation for each case is merely a summation resulting in a single term for each interface pair across the intervening medium layer. The distance part in the denominator is equivalent to the separation distance between that given pair of interfaces. The Hamaker coefficient subscripts denote the optical properties of the two neighboring materials at each of these interfaces using the ordering scheme described above (outermost material gets listed first). Thus each term can easily be constructed from the picture. As an example, the last interfaces in case C3 have a Hamaker coefficient $\mathcal{A}_{mv/vh}$ at an interface-interface separation distance of $\ell+a$. It is worth noting that in cases such as C2, the Hamaker coefficients are equal in magnitude but opposite in sign simply because they include the same spectra and just have their subscript order reversed. If we were to bring these interfaces completely together, the two total energy terms would cancel out as expected because the interfaces would annihilate and disappear.

At the near-limit, it is clearly the materials closest to the intervening medium that dominates the total vdW-Ld energy interaction, which is demonstrated by the C1/C2 ratio con-

verging to 1 and thus being effectively equal despite the fact that C2 is of a finite thickness and has an additional interface term. This effective equivalence is due to the divergent, $1/\ell^2$ behavior of the nearest interface-interface pair dominating the total energy as ℓ goes to zero. In effect, one can place any arbitrary number of interfaces at distances well beyond the leading term and they would have little to no impact on the total vdW-Ld energy. Therefore at contact, we only need to use the optical properties of the outermost layer and need not and should not use any spectral mixing.

The opposite effect occurs at the far limit. The individual Hamaker coefficients found in all four terms of case C3 are much larger than the Hamaker coefficients for case C2 because the spectral contrast at each interface in C3 is much greater. One might be too quick to conclude that these larger Hamaker coefficients should lead to a larger total energy for case C3 as compared to C2. However, the interfaces in C3 begin to pack more closely and thus the overall magnitudes of the $1/\ell^2$ terms (i.e., the geometrical components) of the neighboring interfaces get closer. These two effects (increasing Hamaker coefficients and decreased spacing) cancel each other out making cases C2 and C3 nearly identical in the far limit, with case C2 certainly giving us an advantage of reduced complexity.

Figure 9(b) illustrates these effects. Additionally, it is important to note that ratio of C3/C2 converges to a fixed value when $\ell > 2d$, where d is the thickness of the finite layers in cases C3 and C2. This particular distance of convergence is an encouraging result because it is the exact same distance we determined to be far limit regime in our analysis of the anisotropic solid-cylinder Lifshitz formulations. For the purposes of stress-testing the EMA mixing rules, we purposely chose extreme values of s to mimic the vacuum ($v:s=0$) and metal ($h:s=100$) end points. Therefore this 23% discrepancy can be thought of as the maximum error that can exist between the total vdW-Ld energies of cases C2 and C3 in the far limit. If we were to pick values of s that were closer in value to each other (e.g., $v:s=50$ and $h:s=100$), then the difference in the total energy drops to less than 4%. Moreover, of course, if materials v and h have identical spectra, the ratio of C2/C3 merges to unity at the far limit. Therefore one can confidently mix spectra that are on the same order of magnitude and be sure they are getting

realistic results. When spectra are vastly different, there will be some discrepancies that need to be taken into account.

There is one final issue to note in Fig. 9. Although the limiting separation regimes are easy to characterize, there is a transition range between the near and far limits which is harder to define. For those cases, one might best use the interpolation method described previously in order to get a reasonable Hamaker coefficient and total vdW-Ld energy at any separation distance. This process is beyond the scope of this paper, which is primarily focused on the effects of mixing on the limiting behaviors. However, those wishing to know this information within this regime can do so in a reasonably straightforward manner.⁸

- ¹P. Lambin, *C. R. Phys.* **4**, 1009 (2003).
²E. B. Barros, A. Jorio, G. G. Samsonidze, R. B. Capaz, A. G. S. Filho, J. M. Filho, G. Dresselhaus, and M. S. Dresselhaus, *Phys. Rep.* **431**, 261 (2006).
³C. T. White and J. W. Mintmire, *J. Phys. Chem. B* **109**, 52 (2005).
⁴V. N. Popov, *Mater. Sci. Eng., R.* **43**, 61 (2004).
⁵R. F. Rajter, R. H. French, W. Y. Ching, W. C. Carter, and Y. M. Chiang, *J. Appl. Phys.* **101**, 054303 (2007).
⁶J. W. Mintmire and C. T. White, *Synth. Met.* **77**, 231 (1996).
⁷V. N. Popov and L. Henrard, *Phys. Rev. B* **70**, 115407 (2004).
⁸R. F. Rajter, R. Podgornik, V. A. Parsegian, R. H. French, and W. Y. Ching, *Phys. Rev. B* **76**, 045417 (2007).
⁹R. F. Rajter and R. H. French, *J. Phys.: Conf. Ser.* **94**, 012001 (2008).
¹⁰M. Zheng, A. Jagota, M. S. Strano, A. P. Santos, P. Barone, S. G. Chou, B. A. Diner, M. S. Dresselhaus, R. S. Mclean, G. B. Onoa, G. G. Samsonidze, E. D. Semke, M. Usrey, and D. J. Walls, *Science* **302**, 1545 (2003).
¹¹M. Zheng and E. D. Semke, *J. Am. Chem. Soc.* **129**, 6084 (2007).
¹²S. R. Lustig, A. Jagota, C. Khripin, and M. Zheng, *J. Phys. Chem.* **109**, 2559 (2005).
¹³H. Peng, N. Alvarez, C. Kittrell, R. H. Hauge, and H. K. Schmidt, *J. Am. Chem. Soc.* **128**, 8396 (2006).
¹⁴J. Chung, K.-H. Lee, J. Lee, and R. S. Ruoff, *Langmuir* **20**, 2011 (2004).
¹⁵S. Manohar, T. Tang, and A. Jagota, *J. Phys. Chem. C* **111**, 17835 (2007).
¹⁶E. M. Lifshitz, *Sov. Phys. JETP* **2**, 73 (1956).
¹⁷V. A. Parsegian, *Van der Waals Forces* (Cambridge University Press, Cambridge, England, 2005).
¹⁸R. H. French, *J. Am. Ceram. Soc.* **83**, 2117 (2000).
¹⁹K. van Benthem, G. Tan, R. H. French, L. K. Denoyer, R. Podgornik, and V. A. Parsegian, *Phys. Rev. B* **74**, 205110 (2006).
²⁰R. Podgornik, R. H. French, and V. A. Parsegian, *J. Chem. Phys.* **124**, 044709 (2006).
²¹See <http://sourceforge.net/projects/geckoproj> for Gecko Hamaker software.
²²D. A. G. Bruggeman, *Ann. Phys. (N.Y.)* **24**, 636 (1935).
²³Ph. J. Roussel, J. Vanhellefont, and H. E. Maes, *Thin Solid Films* **234**, 423 (1993).
²⁴H. Fujiwara, J. Koh, P. I. Rovira, and R. W. Collins, *Phys. Rev. B* **61**, 10832 (2000).
²⁵W. Y. Ching, *J. Am. Ceram. Soc.* **71**, 3135 (1990).
²⁶R. H. French, S. J. Glass, F. S. Ohuchi, Y. N. Xu, and W. Y. Ching, *Phys. Rev. B* **49**, 5133 (1994).
²⁷W. Y. Ching, Y. N. Xu, and R. H. French, *Phys. Rev. B* **54**, 13546 (1996).
²⁸Y. N. Xu, W. Y. Ching, and R. H. French, *Phys. Rev. B* **48**, 17695 (1993).
²⁹Y. N. Xu and W. Y. Ching, *Phys. Rev. B* **51**, 17379 (1995).
³⁰W. Y. Ching and R. H. French (unpublished correspondence).
³¹H. D. Ackler, R. H. French, and Y. M. Chiang, *J. Colloid Interface Sci.* **179**, 460 (1996).
³²R. R. Dagastine, D. C. Prieve, and L. R. White, *J. Colloid Interface Sci.* **231**, 351 (2000).
³³C. M. Roth and A. M. Lenhoff, *J. Colloid Interface Sci.* **179**, 637 (1996).
³⁴J. M. Fernandez-Varea and R. Garcia-Molina, *J. Colloid Interface Sci.* **231**, 394 (2000).
³⁵R. H. French, K. I. Winey, M. K. Yang, and W. Qiu, *Aust. J. Chem.* **60**, 251 (2007).
³⁶Y. Li, S. V. Rotkin, and U. Ravaioli, *Nano Lett.* **3**, 183 (2003).
³⁷Y. Li, S. V. Rotkin, and U. Ravaioli, *Appl. Phys. Lett.* **85**, 4178 (2004).
³⁸Y. Li, U. Ravaioli, and S. S. V. Rotkin, *Phys. Rev. B* **73**, 035415 (2006).
³⁹Y. Li, S. V. Rotkin, and U. Ravaioli, *Proc. IEEE Nanotechnol.* **3**, 1 (2003).
⁴⁰R. R. Dagastine, D. C. Prieve, and L. R. White, *J. Colloid Interface Sci.* **249**, 78 (2002).
⁴¹*Handbook of Optical Constants of Solids*, edited by E. D. Palik (Academic, New York, 1985), Vol. I; *Handbook of Optical Constants of Solids*, edited by E. D. Palik (Academic, New York, 1991), Vol. II; *Handbook of Optical Constants of Solids*, edited by E. D. Palik (Academic, New York, 1998), Vol. III.